Supporting Information

Jenner et al. 10.1073/pnas.1216691110

SI Materials and Methods

Reagents. Tetracycline (EMD Biosciences) and tigecycline (Sigma) were purchased from commercial sources, whereas PTK0796, TP767, pentacycline (TP556D) and azacycline (TP120C) were provided by Tetraphase. [^{3}H]Tetracycline was purchased from Perkin-Elmer. Ribosomes from *Thermus thermophilus* cells were isolated as described previously (1, 2). Purified native uncharged *Escherichia coli* tRNA^{fMet} was supplied by Chemical Block. The 30-nt-long mRNA [5′-GGCAAGGAGGUAAAA AUG UAC $(A)_6$-3′] was purchased from Dharmacon (Shine–Dalgarno sequence and initiation codon are underlined). Recombinant purified TetM protein was prepared as described previously (3).

Complex Formation and Crystallization. The ribosomal complexes were formed in 10 mM Tris-Acetate, pH 7.0, 40 mM KCl, 7.5 mM magnesium acetate, 0.5 mM DTT by incubating 70S ribosomes (3 μM) with mRNA, tRNA^{fMet}, and antibiotic (tetracycline or tigecycline) for 30 min at 37 °C. Crystals were grown at 24 °C by sitting-drop vapor diffusion based on the previously described procedure (2). At first, tigecycline and tetracycline in their respective complexes were used in 20-fold excesses (60 μM final) of the ribosome and tRNA^{fMet} in fivefold excess. Structure analysis showed a single binding site for tigecycline in both ribosomes in the asymmetric unit. In contrast, analysis of the ribosome complexes cocrystallized with tetracycline (in 20-fold stoichiometric excess) showed no drug bound to the ribosome. This crystal form ($P2_12_12_1$) contains two ribosome molecules per asymmetric unit (termed molecule A and molecule B). As a result of crystal packing, some peripheral parts are slightly different between the two molecules, but the core part of the ribosome remains the same. Molecule A is almost always better defined in the electron density, and therefore most interpretations are based on this molecule. In a previous study (2), we observed that the "initiation" complex formed with *T. thermophilus* 70S ribosomes cocrystallized with mRNA and tRNA^{fMet} in conditions similar to the one used in the present study, which contains tRNA^{fMet} in P- and E-sites of both ribosomes in the asymmetric unit. However, the A site was occupied by noncognate tRNA^{fMet} in molecule A, whereas molecule B had an empty A site. The negative result from the tetracycline data demonstrates that, at the concentration and stoichiometric ratio used (60 μM; 20:1), tetracycline has much lower binding affinity than tigecycline, which was able not only to bind to the unoccupied A-tRNA site in molecule B, but also to compete with noncognate initiator tRNA^{fMet} (which was present in fivefold excess) for the binding to the A site in molecule A. To achieve full binding of tetracycline in molecules A and B, we had to lower the stoichiometric excess of tRNA^{fMet} to 1.5 and increase the excess of tetracycline to 100 times (300 μM final) the ribosome concentration.

Data Collection, Processing, and Structure Determination. Data on all complexes were collected at 100 K at the Swiss Light Source, PSI, using the Pilatus 6M detector. A very low dose mode was used, and huge redundancy was collected (4). The initial model (from ref. 5, with tRNAs, mRNA, and metal ions removed) was correctly placed within each data set with Phenix (6) by rigid body refinement with each molecule defined as a rigid body. This was followed by rigid body refinement of individual subunits. After positional and B-factor refinement, the tRNAs and mRNA and were built in these unbiased electron density maps. In a subsequent round, the difference F_{obs}–F_{calc} electron density maps were inspected for possible locations of antibiotics, which were then built into the density (Figs. S2 and S6). Electron density for tigecycline and tetracycline was only observed at a single binding site (corresponding to the previously determined primary tetracycline binding site) and not at any of the previously reported secondary tetracycline binding sites (7, 8) (Fig. S1). Moreover, crystallization of the 70S complex was performed in the presence of higher concentrations (300 μM) of tetracycline than used previously (4–80 μM). After several cycles of manual rebuilding followed by positional and individual isotropic B-factor refinement, magnesium ions were added. Apart from the structural magnesium coordinated by the phosphate oxygen atoms of C1054, G1197, and G1198 from helix 34 of 16S rRNA and the hydrophilic side of the tetracyclines, we found indications of a second magnesium involved in coordination of tetracycline antibiotics. This second putative magnesium is most strongly seen for the tigecycline complex (Fig. S1), where it makes salt bridges with the phosphate oxygen atoms of G966 from helix 31 and the OH group at position 3 in ring A. In the tetracycline structure, the presence of this magnesium is much less obvious (Fig. S4), possibly because of lower occupancy of the site or lower resolution of the data. However, when removing it from the tetracycline complex model, this magnesium repeatedly reappears in unbiased omit-averaged kick maps (9). A summary of the crystallographic data and refinement statistics is given in Table S1.

Aminoacylation and Fluorescent Labeling of tRNA for Single-Molecule Fluorescence. tRNA^{fMet} and tRNA^{Phe} from *E. coli* strain MRE600 were obtained from commercial sources (Sigma). Aminoacylation, formylation, and fluorescent labeling of tRNA were performed as previously described (10). By using this approach, Cy3 and Cy5 dyes (GE Healthcare) were site-specifically attached through maleimide or *N*-hydroxysuccinimide chemistry to tRNA^{fMet}(s^4U8) and tRNA^{Phe}(acp^3U47) at naturally occurring modified base residues located near the elbow region of the tRNA body. Charging of tRNA^{Phe} was achieved by using recombinant phenylalanyl tRNA synthetase prepared as previously described (10–12). Dye-labeled tRNAs prepared in this manner are fully competent in tRNA selection, translocation, and peptide bond formation (10).

Preparation of Ribosome Complexes for Single-Molecule Fluorescence. The 30S and 50S ribosomal subunits were isolated from *E. coli* strain BL21(DE3) as previously described (12). Initiation complexes were prepared by using purified 50S and 30S subunits (1 μM each) initiated in vitro on 5′-biotinylated gene 32-derived mRNA (5′-biotin-CAA CCU AAA ACU UAC ACA CCC UUA GAG GGA CAA UCG AUG UUC AAA GUC UUC AAA GUC AUC; Dharmacon) in the presence of IF-1 (2 μM), IF-2 (2 μM), IF-3 (2 μM), 2 mM GTP, and fMet-tRNA^{fMet} (Cy3-s^4U8) in Tris-polymix buffer (pH 7.5) containing 50 mM Tris acetate, pH 7.5, 5 mM $Mg(OAc)_2$, 100 mM KCl, 5 mM NH_4OAc, 0.5 mM $CaCl_2$, 0.1 mM EDTA, 5 mM putrescine, and 1 mM spermidine as previously described (10).

Single-Molecule Fluorescence Experiments and Data Processing. All experiments were performed in Tris-polymix buffer (pH 7.5) containing 50 mM Tris acetate, pH 7.5, 15 mM MgOAc, 100 mM KCl, 5 mM NH_4OAc, 0.5 mM $CaCl_2$, 0.1 mM EDTA, 5 mM putrescine, 1 mM spermidine, 5 mM β-mercaptoethanol, and 100 μM GTP, in the presence of an oxygen scavenging environment (2 mM protocatechuic acid and 50 nM protocatechuate-3,4-dioxygenase) containing a mixture of triplet-state quenching

compounds (1 mM Trolox, 1 mM cyclooctatetraene, 1 mM nitrobenzyl alcohol) (13). Ternary complex of elongation factor thermo unstable·GTP·Phe-tRNA^{Phe}(Cy5-acp^{3}U47) was prepared following established procedures (10, 12). Ribosome complexes (0.5 nM) programmed with biotinylated mRNA were surface-immobilized following brief incubation within PEG-passivated, streptavidin-coated quartz microfluidic devices (12). To avoid contributions of hybrid states formation following accommodation, the amino acid on P-site tRNA was released by incubating immobilized ribosomes with 2 mM puromycin (Sigma), pH 8.5, for 10 min.

Single-molecule fluorescence resonance energy transfer (FRET) data were acquired by using a prism-based total internal reflection microscope as previously described (12). The Cy3 fluorophore linked to tRNA^{fMet} was excited by the evanescent wave generated by total internal reflection of a single-frequency light source (532 nM; Ventus; Laser Quanta). Photons emitted from Cy3 and Cy5 were collected by using a 1.2 NA, 60× water-immersion objective (Nikon), with optical treatments used to spatially separate Cy3 and Cy5 frequencies onto a cooled, back-thinned electron-multiplying CCD camera (Evolve 512; Photometrics). Fluorescence data were acquired by using MetaMorph acquisition software (Universal Imaging) with an integration time of 200 ms. FRET trajectories were calculated from fluorescence trajectories by using the following formula: $FRET = I_{Cy5} / (I_{Cy3} + I_{Cy5})$, where I_{Cy3} and I_{Cy5} represent the Cy3 and Cy5 fluorescence intensities, respectively. In each experiment, ternary complex solution was rapidly exchanged after ~5 s of imaging.

Fluorescence and FRET traces were selected for analysis by using semiautomated single-molecule FRET analysis software implemented in Matlab (MathWorks) with use of the following criteria: a single catastrophic photobleaching event, total (donor plus acceptor) fluorescence intensity within 2 SDs of the mean, at least 8:1 signal-to-background noise ratio, fewer than four donor fluorophore blinking events, and a donor lifetime of at least 500 frames (100 s). FRET trajectories were idealized by using the segmental *k*-means algorithm (14) and a three-state, linear starting model with E_{FRET} fixed as follows: 0.01 ± 0.061, 0.25 ± 0.08, and 0.56 ± 0.15. Each ribosome was assumed to have accommodated when a continuous dwell in the high FRET state was observed for at least 1 s (five frames).

***E. coli*-Coupled in Vitro Transcription/Translation Assay.** Inhibitory activity of the tetracycline compounds was assessed in an *E. coli*-coupled in vitro transcription/translation assay (5 PRIME) using GFP fluorescence as a read-out, as described previously (15, 16). Serial dilutions spanning the activity range of each compound, 0.01 to 100 μM were performed, with the addition of 0.5 μM recombinant TetM protein when required. Reaction mixtures were performed in a total volume of 5 μL for 3 h at 30 °C and stopped by placing on ice for 5 min. Subsequently, each reaction was diluted with 50 μL of buffer A (10 mM Hepes/KOH, pH 7.8, 10 mM $MgCl_2$, 60 mM NH_4Cl, 4 mM β-mercaptoethanol), mixed, and then transferred into black 96-well chimney plates (Greiner). The GFP fluorescence was measured on a Tecan Infinite M1000 reader with an excitation wavelength of 395 nm and emission of 509 nm. The results were represented graphically by using SigmaPlot (Systat).

[^{3}H]Tetracycline Competition Assay. Binding of all tetracycline compounds to 70S ribosomes was examined by using a competition assay as described previously (17). Briefly, all reaction mixtures contained 0.4 μM *E. coli* 70S ribosomes and 8 μM [^{3}H]tetracycline in binding buffer (10 mM Hepes/KOH, pH 7.8, 30 mM $MgCl_2$, 150 mM NH_4Cl, 6 mM β-mercaptoethanol), which equated to 80% binding from the saturation curve. To measure the IC_{50} for each of the compounds, reactions were performed in the absence or presence of increasing concentrations of the competing compounds. All compounds were tested at concentrations ranging from 0.01 to 10 μM, whereas tetracycline was tested at concentrations ranging from 0.01 to 75 μM. After incubation at room temperature for 2 h, reactions were passed through nitrocellulose filters, type HA, with 0.45-μm pore size (Millipore). Filters were washed three times with binding buffer, and radioactivity was determined by using a scintillation counter in the presence of Filtersafe (Zinsser Analytic) scintillant. Results presented are averages from at least two independent experiments.

1. Gogia ZV, Yusupov MM, Spirina TN (1986) Structure of Thermus thermophilus ribosomes. Method of isolation and purification of ribosomes. *Molekul Biol (USSR)* 20:519–526.
2. Jenner LB, Demeshkina N, Yusupova G, Yusupov M (2010) Structural aspects of messenger RNA reading frame maintenance by the ribosome. *Nat Struct Mol Biol* 17(5):555–560.
3. Mikolajka A, et al. (2011) Differential effects of thiopeptide and orthosomycin antibiotics on translational GTPases. *Chem Biol* 18(5):589–600.
4. Mueller M, Wang M, Schulze-Briese C (2012) Optimal fine φ-slicing for single-photon-counting pixel detectors. *Acta Crystallogr D Biol Crystallogr* 68(pt 1):42–56.
5. Demeshkina N, Jenner L, Westhof E, Yusupov M, Yusupova G (2012) A new understanding of the decoding principle on the ribosome. *Nature* 484(7393):256–259.
6. Afonine PV, et al. (2012) Towards automated crystallographic structure refinement with phenix.refine. *Acta Crystallogr D Biol Crystallogr* 68(pt 4):352–367.
7. Brodersen DE, et al. (2000) The structural basis for the action of the antibiotics tetracycline, pactamycin, and hygromycin B on the 30S ribosomal subunit. *Cell* 103(7):1143–1154.
8. Pioletti M, et al. (2001) Crystal structures of complexes of the small ribosomal subunit with tetracycline, edeine and IF3. *EMBO J* 20(8):1829–1839.
9. Prażnikar J, Afonine PV, Guncar G, Adams PD, Turk D (2009) Averaged kick maps: Less noise, more signal... and probably less bias. *Acta Crystallogr D Biol Crystallogr* 65(pt 9):921–931.
10. Blanchard SC, Gonzalez RL, Kim HD, Chu S, Puglisi JD (2004) tRNA selection and kinetic proofreading in translation. *Nat Struct Mol Biol* 11(10):1008–1014.
11. Blanchard SC, Kim HD, Gonzalez RL, Jr., Puglisi JD, Chu S (2004) tRNA dynamics on the ribosome during translation. *Proc Natl Acad Sci USA* 101(35):12893–12898.
12. Munro JB, Altman RB, O'Connor N, Blanchard SC (2007) Identification of two distinct hybrid state intermediates on the ribosome. *Mol Cell* 25(4):505–517.
13. Dave R, Terry DS, Munro JB, Blanchard SC (2009) Mitigating unwanted photophysical processes for improved single-molecule fluorescence imaging. *Biophys J* 96(6):2371–2381.
14. Qin F (2004) Restoration of single-channel currents using the segmental k-means method based on hidden Markov modeling. *Biophys J* 86(3):1488–1501.
15. Starosta AL, et al. (2009) Identification of distinct thiopeptide-antibiotic precursor lead compounds using translation machinery assays. *Chem Biol* 16(10):1087–1096.
16. Starosta A, et al. (2010) Interplay between the ribosomal tunnel, nascent chain, and macrolides influences drug inhibition. *Chem Biol* 17:1–10.
17. Grossman TH, et al. (2012) Target- and resistance-based mechanistic studies with TP-434, a novel fluorocycline antibiotic. *Antimicrob Agents Chemother* 56(5):2559–2564.

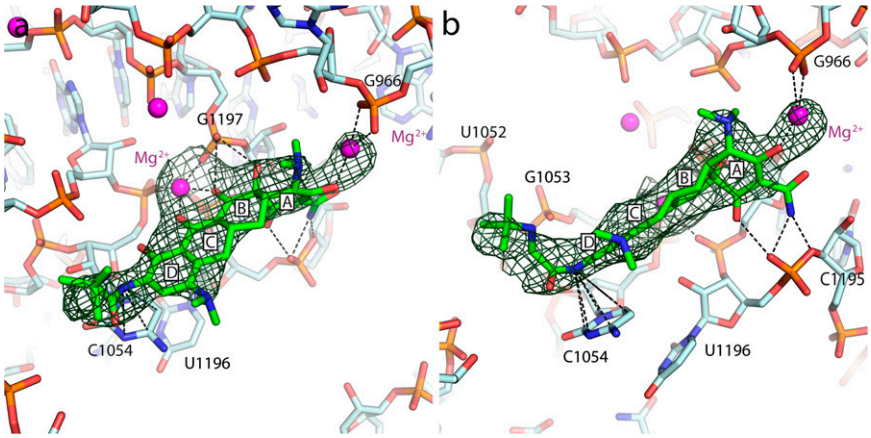

Fig. S1. $F_{obs}-F_{calc}$ difference map for tigecycline. (*A* and *B*) Two different views of the original $F_{obs}-F_{calc}$ electron density map calculated before tigecycline was added to the model, contoured at 3 sigma. This completely unbiased map unambiguously shows the position of the antibiotic as well as the secondary magnesium ion (coordinated by G966). The first magnesium, which is a magnesium ion important for the structural integrity of the region and is always there regardless of antibiotics and ligands, shows up in this map because it was removed from the model before map calculation.

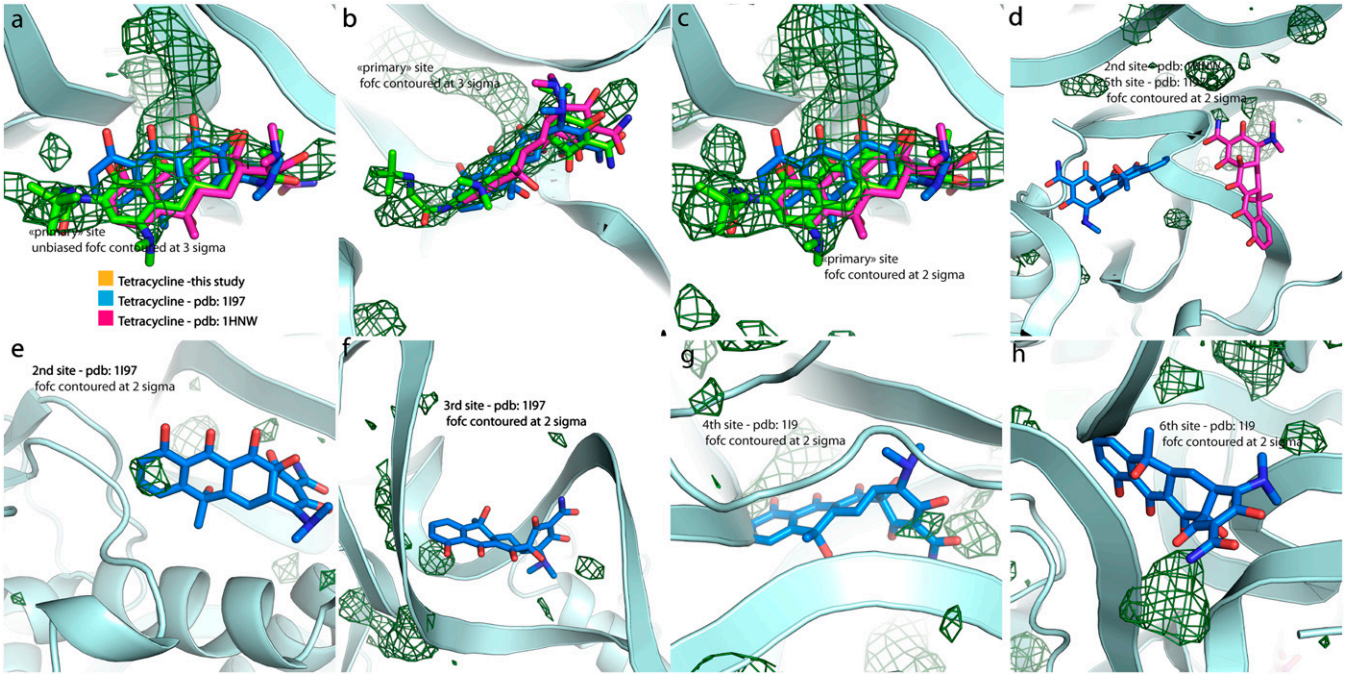

Fig. S2. Lack of density for tigecycline at secondary tetracycline binding sites. Unbiased $F_{obs}-F_{calc}$ difference electron density map contoured at 3 sigma for the sole tetracycline binding site found in this study. (*A* and *B*) This site corresponds to the "primary" tetracycline binding site found in two previous studies (1, 2). (*C*) The same map as in *A*, but contoured at 2 sigma, which is generally considered very low for a $F_{obs}-F_{calc}$ map. (*D*) The "secondary" binding site [Protein Data Bank (PDB) ID: 1HNW (ref. 1)] and "fifth" binding site [PDB ID: 1I97 (ref. 2)] for tetracycline found in the previous studies based on isolated 30S subunit soaked with tetracycline shown with our $F_{obs}-F_{calc}$ map contoured at 2 sigma. Clearly, in our study, no tigecycline is bound at this site. (*E–H*) The remaining four binding sites located in one of the previous studies (1). [A total of six tetracycline sites was found with only one (the "primary") having full occupancy.] Again, our maps clearly show that there is no antibiotic bound at these sites. In many cases, these "extra sites" are located in grooves of RNA that are well known for binding various ions or in areas that are very flexible with poorly defined electron density. Taken together with the data resolution and quality, it is therefore plausible that electron density for ions or extra electron density arising from poorly modeled areas could have been misinterpreted as bound antibiotics.

1. Brodersen DE, et al. (2000) The structural basis for the action of the antibiotics tetracycline, pactamycin, and hygromycin B on the 30S ribosomal subunit. *Cell* 103(7):1143–1154.
2. Pioletti M, et al. (2001) Crystal structures of complexes of the small ribosomal subunit with tetracycline, edeine and IF3. *EMBO J* 20(8):1829–1839.

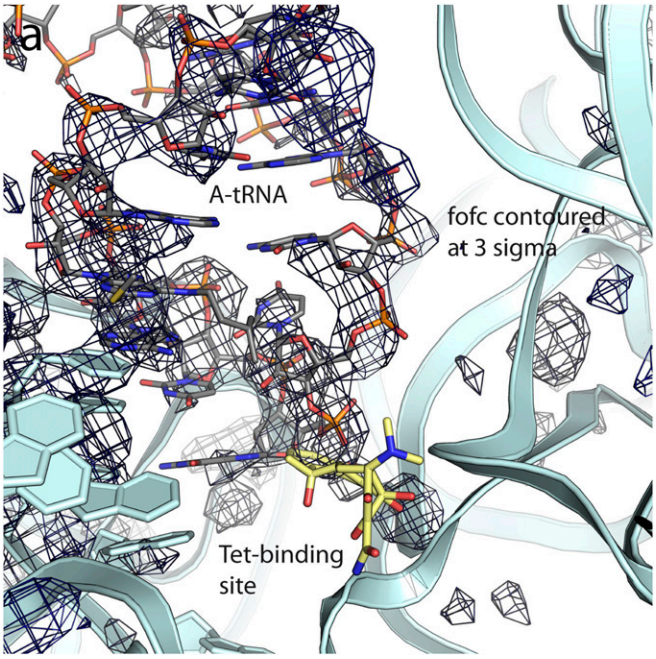

Fig. S3. $F_{obs}-F_{calc}$ difference map for calculated for data collected on crystals cocrystallized in 20 μM tetracycline. The original $F_{obs}-F_{calc}$ electron density map contoured at 3 sigma and calculated before any ligands (antibiotics, tRNAs, mRNAs) were added to the model. The presence of electron density for A-tRNA, but not for tetracycline, demonstrates that tetracycline at these conditions is not capable of competing with $tRNA^{fMet}$ for binding to the A site.

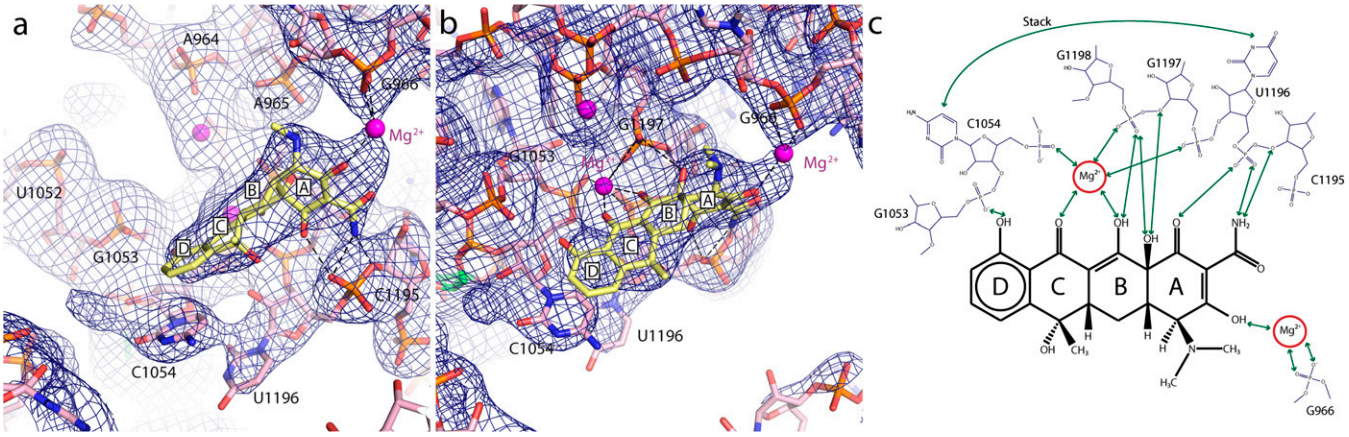

Fig. S4. The tetracycline binding site. (*A* and *B*) The fully refined $2F_{obs}-F_{calc}$ electron density map contoured at 1.2 sigma for the area surrounding the binding site of tetracycline (yellow). (*C*) Schematic chemical structure of tetracycline showing possible hydrogen bonds and other interactions with Mg^{2+} ions and bases from 16S rRNA.

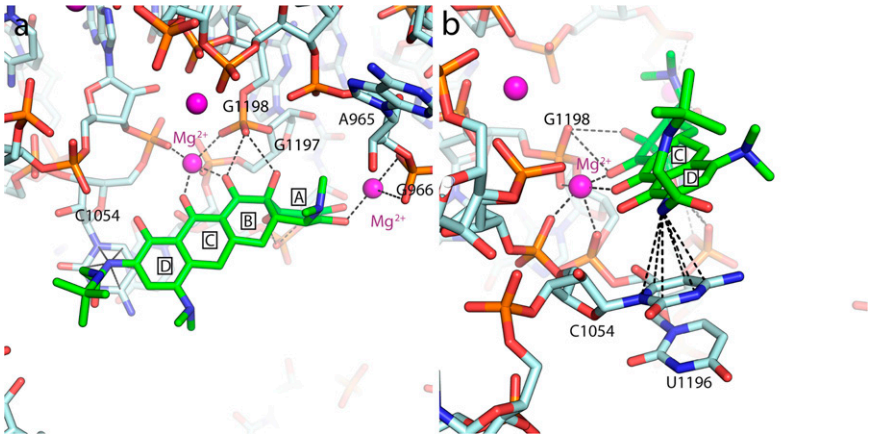

Fig. S5. The tigecycline binding site. (*A* and *B*) Two different orientations showing the binding mode of tigecycline. Possible hydrogen bonds and other interactions are indicated.

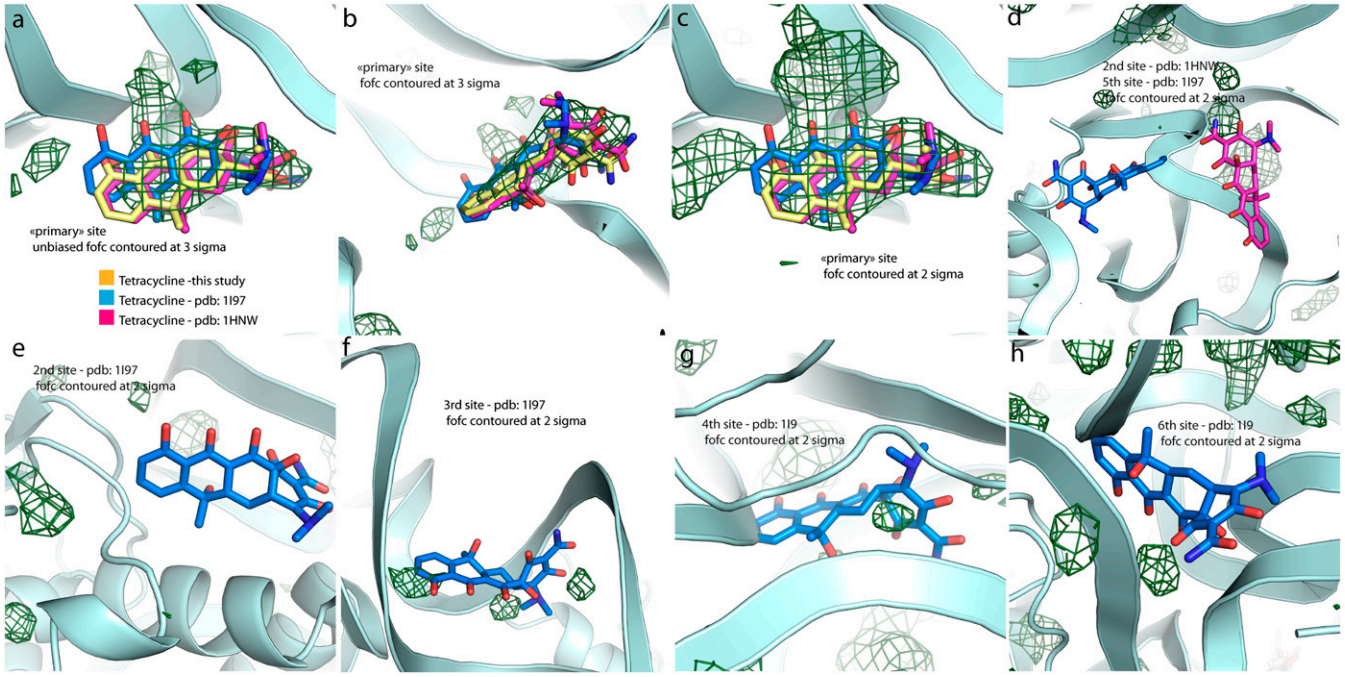

Fig. S6. Lack of density for tetracycline at secondary tetracycline binding sites. (*A* and *B*) Unbiased F_{obs}–F_{calc} difference electron density map contoured at 3 sigma for the sole tetracycline binding site found in this study. This site corresponds to the primary tetracycline binding site found in two previous studies (1, 2). (*C*) The same map as in *A*, but contoured at 2 sigma, which is generally considered very low for a F_{obs}–F_{calc} map. (*D*) The secondary binding site [PDB ID: 1HNW (ref. 1)] and fifth binding site [PDB ID: 1I97 (ref. 2)] for tetracycline found in the previous studies based on isolated 30S subunit soaked with tetracycline shown with our F_{obs}–F_{calc} map contoured at 2 sigma. Clearly, in our study, no tetracycline is bound at this/these site(s). (*E*–*H*) The remaining four binding sites located in one of the previous studies (2). [A total of six tetracycline sites was found with only one (the primary) having full occupancy.] Again, our maps clearly show that there is no antibiotic bound at these sites. In many cases, these extra sites are located in grooves of RNA that are well known for binding various ions or in areas that are very flexible with poorly defined electron density. Taken together with the data resolution and quality, it is therefore plausible that electron density for ions or extra electron density arising from poorly modeled areas could have been misinterpreted as bound antibiotics.

1. Brodersen DE, et al. (2000) The structural basis for the action of the antibiotics tetracycline, pactamycin, and hygromycin B on the 30S ribosomal subunit. *Cell* 103(7):1143–1154.
2. Pioletti M, et al. (2001) Crystal structures of complexes of the small ribosomal subunit with tetracycline, edeine and IF3. *EMBO J* 20(8):1829–1839.

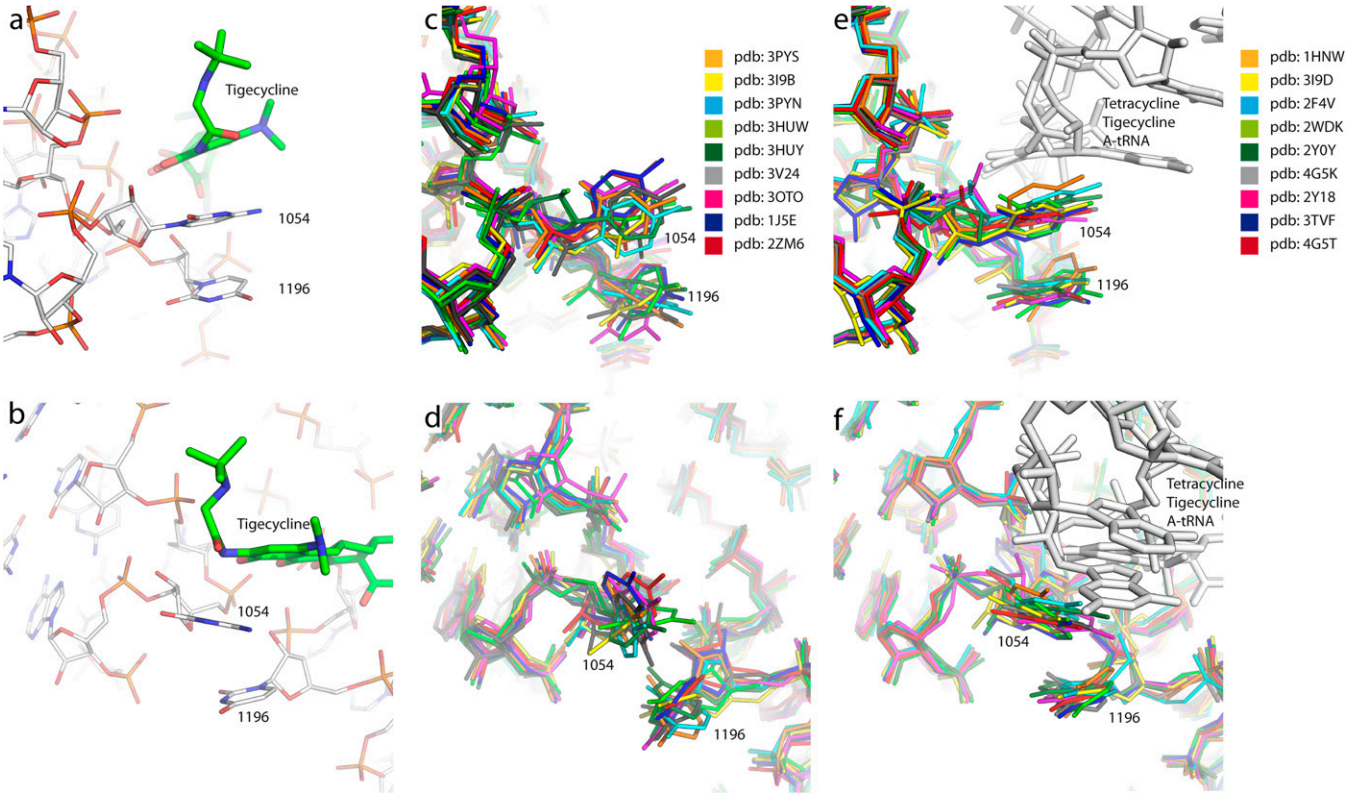

Fig. S7. Behavior of nucleotides C1054 and U1196. (*A* and *B*) Two different orientations showing the orientations of the two nucleotides (C1054 and U1196) that stack with the 9-t-butylglycylamido moiety of tigecycline (green). (*C* and *D*) A superposition of structures of 70S (PDB IDs: 3PYS, 3I9B, 3PYN, 3HUW, 3HUY, 3V24) and isolated 30S (PDB IDs: 3OTO, 1J5E, 2ZM6) with an empty A site. This comparison illustrates that the nucleotides 1054 and 1196 are rather flexible and can take on several positions when the A site is unoccupied. (*E* and *F*) superposition of structures of 70S (PDB IDs: 3I9D, 2WDK, 2Y0Y, 4F5K, 2Y18, 3TVF, 4G5T) and isolated 30S (PDB IDs: 1HNW, 2F4V) with an A-site ligand (antibiotics or tRNAs). In contrast to *C* and *D*, the nucleotides C1054 and U1196 tend to become ordered when A-site ligands bind. It should be noted that these nucleotides being pyrimidines are easy to misrefine, as most refinement programs do not take π-stacking into account but mostly try to avoid stereochemical clashes.

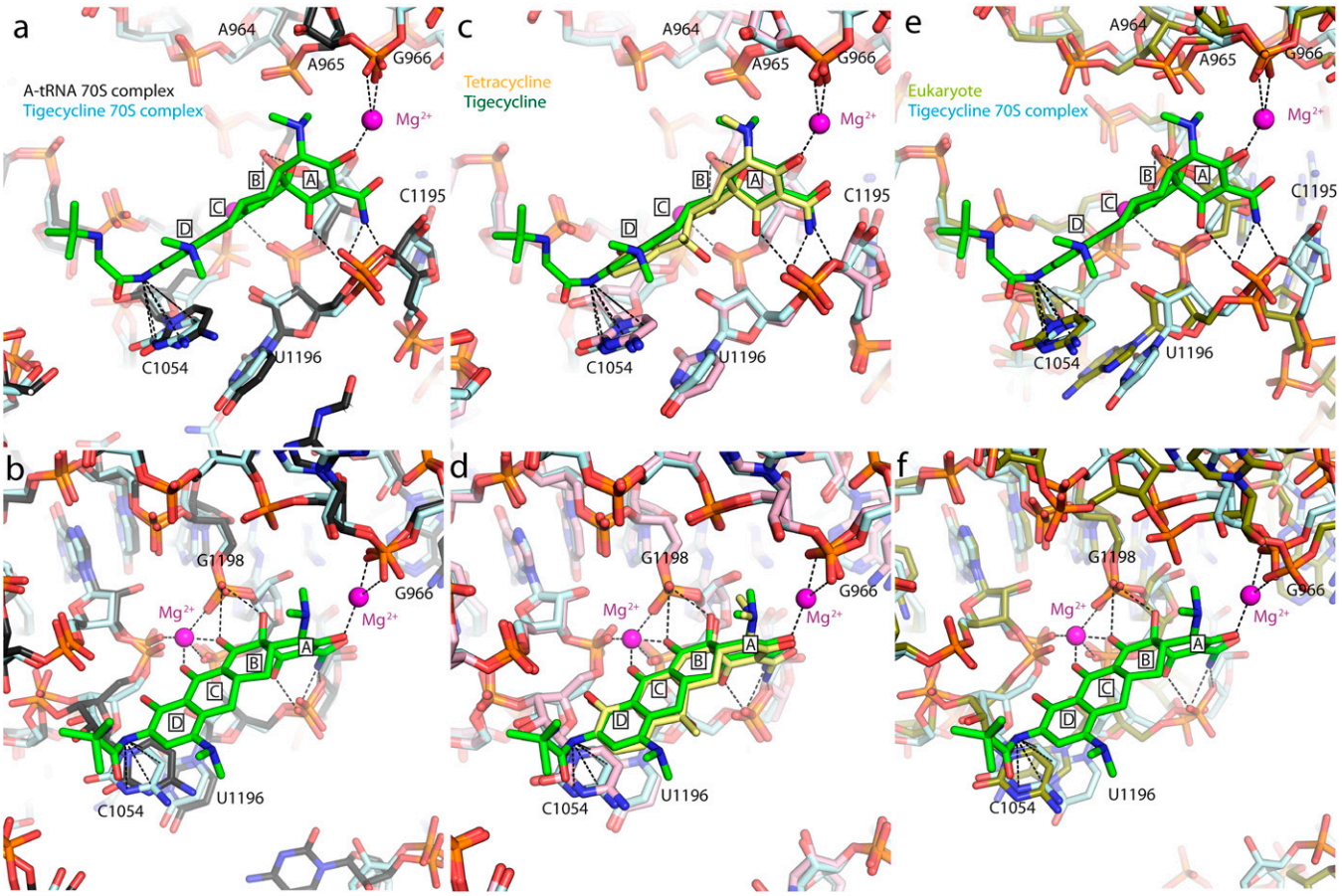

Fig. S8. Comparisons of the tetracycline binding pocket. (*A* and *B*) Comparison of the antibiotic binding area of the 70S complex with tigecycline (16S rRNA in cyan) or with A-tRNA (16S rRNA in black; PDB ID: 3UZ6). Only a small difference in the orientation of nucleotide C1054 is observed, which seems to slightly adjust its position according to the ligand bound, whereas the rest of the pocket is identical between the two complexes. (Note: The A-tRNA was removed for clarity.) (*C* and *D*) Comparison of the 70S complexes with tigecycline (tigecycline in green, 16S RNA in cyan) and tetracycline (tetracycline in yellow, 16S rRNA in pink). These antibiotics are coordinated in the same way, and there is no significant difference in the binding pocket. The substitution at the 9-position of tigecycline enhances the stacking effect with C1054, but the orientation of these "stacking" nucleotides (C1054 and U1196) is the same for both antibiotic agents. (*E* and *F*) Comparison of the *T. thermophilus* 70S ribosome complex with tigecycline (tigecycline in green, 16S RNA in cyan) and the eukaryotic *Saccharomyces cerevisiae* 80S ribosome (18S rRNA in green/gold; PDB ID: 3U5B). In *S. cerevisiae*, an adenine is at the position corresponding to U1196; however, most of the tetracycline binding pocket is highly conserved, and, from the superposition, we see that this conservation is also true structurally. Slight shifts in helix 31 (h31) and helix 34 (h34) may be a result of the rotated state of the eukaryotic 80S ribosome (1).

1. Ben-Shem A, et al. (2011) The structure of the eukaryotic ribosome at 3.0 Å resolution. *Science* 334(6062):1524–1529.

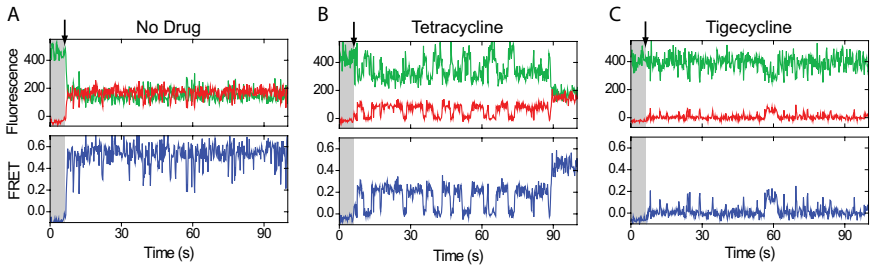

Fig. S9. Effect of tetracycline and tigecycline on tRNA selection as measured by using single-molecule FRET. Representative single-molecule fluorescence (donor in green, acceptor in red) and FRET (blue) traces of tRNA selection (as in Fig. 3) are shown for experiments performed (*A*) in the absence of drugs, (*B*) with 40 μM tetracycline, and (*C*) with 2 μM tigecycline. Arrows indicate injection of ternary complex and the start of the tRNA accommodation process.

Table S1. Data collection and refinement statistics

	70S·tigecycline	70S·tetracycline
Data collection		
Space group	$P2_12_12_1$	$P2_12_12_1$
Cell dimensions		
a, *b*, *c*, Å	210.1, 450.3, 616.9	209.3, 448.5, 615.8
α, β, γ, °	90.0, 90.0, 90.0	90.0, 90.0, 90.0
Resolution, Å	300–3.2 (3.3–3.2)*	300–3.3 (3.45–3.3)
R_{merge}	0.21	0.18
$I/\sigma I$	10.5 (1.4)†	10.7 (1.7)
Completeness, %	99.9 (99.8)	100.0 (100.0)
Redundancy	45 (42)	45 (43)
Refinement		
Resolution, Å	300–3.2	300–3.3
No. reflections	1,056,765	859,870
R_{work}/ R_{free}	0.21/0.27	0.20/0.25
No. of atoms		
Protein/RNA	295,879	292,494
B-factors		
Protein/RNA	111.6	135.6
rmsds		
Bond lengths, Å	0.008	0.005
Bond angles, °	1.015	0.682
ML estimate of coordinate error, Å	0.36‡	0.27
PDB code, 30S/50S	4G5T/4G5U	4G5K/4G5L

Three and two crystals, respectively, were used to collect the data. ML, maximum likelihood; PDB, Protein Data Bank.

*Highest resolution shell is shown in parenthesis.

†$I/\sigma I$ of 2.0 at 3.3 Å and 3.45 Å, respectively, for the two datasets.

‡Source: Phenix (1).

1. Afonine PV, et al. (2012) Towards automated crystallographic structure refinement with phenix.refine. *Acta Crystallogr D Biol Crystallogr* 68(pt 4):352–367.